This article has been accepted for publication in IEEE Journal of Selected Topics in Applied Earth Observations and Remote Sensing. This is the author's version which has not been fully e
content may change prior to final publication. Citation information: DOI 10.1109/JSTARS.2024.3381792

Improving GNSS meteorology by fusing measurements of several co-located receivers on the observation level

Rui Wang, Grzegorz Marut, Tomasz Hadaś and Thomas Hobiger

***Abstract*—Zenith Wet Delay (ZWD) estimation is a key component for the Global Navigation Satellite System (GNSS) meteorology. At present, the Zenith Hydrostatic Delay (ZHD) can be computed with sufficient accuracy by means of empirical models, while the ZWD, which is induced by water vapor with the nature of highly spatio-temporal variability, is typically estimated as an unknown parameter in Precise Point Positioning (PPP). Due to GNSS receiver noise and the system biases of GNSS receivers, the accuracy as well as the precision of ZWD estimates is limited. In this study, we propose a novel fusion model based on undifferenced GNSS pseudorange and carrier-phase observations for sites, which have several receivers connected to a single antenna or which are separated horizontally by only a few meters. By fusing GNSS measurements collected by multiple receivers on the observation level, our model can provide common ZWD estimates with a high temporal resolution which can then be used for more accurate and reliable meteorologic applications on a local scale. According to results with simulated and real data, it is revealed that such combined ZWD estimates are superior to single receiver estimates in terms of precision and accuracy. On the other hand, it is confirmed that the estimation of a common ZWD parameter leads to an improvement in positioning accuracy and precision, especially in the vertical component.**

***Index Terms*—Tropospheric delay, Zenith Wet Delay (ZWD), fusion, Precise Point Positioning (PPP), Extended Kalman Filter (EKF).**

I. Introduction

TROPOSPHERIC delays occur when Global Navigation Satellite System (GNSS) signals are travelling from the satellite antenna to the receiver's antenna. A GNSS slant total delay (STD) is caused by the refractive effect of the neutral atmosphere, and consists of two components: the Slant Hydrostatic Delay (SHD) and the Slant Wet Delay (SWD) [1]. Considering that water vapor and the dry gases are contributing as separate components along the propagation path [2], SHD and SWD can be transferred into the zenith direction by using hydrostatic and wet mapping functions, which allow to represent delay in the form of the Zenith Hydrostatic Delay (ZHD) and the Zenith Wet Delay (ZWD), respectively [3], [4]. The ZHD accounts for approximately 90% of the Zenith Total Delay (ZTD) [5], ranging from 2.0 to 2.3 m at sea level [6], and can be well modeled from surface meteorological data. Despite that the ZWD contributes only about 10% to the ZTD, it depends on the water vapor content in the atmosphere, and thus changes rapidly in both spatial and temporal domains. In such case, the ZWD is commonly estimated as an unknown parameter in GNSS data processing [7].

Since the ZWD is nearly proportional to the Precipitable Water Vapor (PWV) above receiver sites [8]–[10], the ZWD estimates have a great potential to be exploited for meteorological applications. The possibilities of using ZWD derived from GNSS for remote sensing of atmospheric water vapor and studies of climate change have been discussed for example by Bevis et al. [10], [11]. Compared to traditional meteorological sensors for atmospheric water vapor measurement like the radiosonde and the Microwave Radiometer (MWR), GNSS can operate in all-weather conditions as well as provide a good spatial and temporal coverage [12], [13]. Various studies have demonstrated that GNSS observations can provide accurate estimates comparable to the measurements of traditional PWV sensors in both post-processing and Near Real-Time (NRT) modes [14]–[16]. The positive impact of assimilating GNSS-derived ZWD in Numerical Weather Prediction (NWP) models has also been investigated during many regional and national projects [16], [17]. Among those projects, a notable example is the EUMETNET EIG GNSS water vapour programme (E-GVAP, http://egvap.dmi.dk/). It was established to further outcomes of the EU COST Action 716, which is a European research project for operational meteorology [13]. In addition, the E-GVAP network data from more than 3500 GNSS sites are processed in NRT to provide GNSS delay and water vapour estimates for use in weather forecasting [18], [19].

In general, GNSS ZTD/PWV estimation is performed either by the network approach using double-differenced observations [14], [16], [20], [21] or the Precise Point Positioning (PPP) [22] approach using undifferenced observations [16], [21], [23]. The advantage of the network approach is that it can effectively cancel out the clock errors and partial orbit errors in the double-differencing process, nevertheless it can be time-consuming, especially in the case of processing GNSS data from a large number of stations [13], [24]. Compared to that, PPP enables the independent and flexible data processing with a single receiver [25]. Furthermore, owing to the development of the International GNSS Service (IGS) Real-Time Service (RTS, http://www.igs.org/rts/), PPP with unlimited coverage can be widely utilized in nowcasting meteorological applications [7]. Our work exploits the PPP approach to GNSS meteorology using undifferenced and uncombined

Rui Wang and Thomas Hobiger are with the Institute of Navigation, University of Stuttgart, Stuttgart, Germany (email: rui.wang@ins.uni-stuttgart.de; thomas.hobiger@ins.uni-stuttgart.de)

Grzegorz Marut and Tomasz Hadaś are with the Institute of Geodesy and Geoinformatics, Wrocław University of Environmental and Life Sciences, Wrocław, Poland (email: grzegorz.marut@upwr.edu.pl; tomasz.hadas@upwr.edu.pl)

observations. Differing from the traditional ionosphere-free combination model, the uncombined PPP model preserves all the information in the observation equations, and hence has the advantage of being able to extract ionospheric delays and easily extended to any number of frequencies [26]–[28].

Though the ZWD is less accurately predictable due to its highly variability, it is unlikely to change significantly over a short period of 10 minutes or less [10]. In a limited or small region, the ZWD is even prone to be stable due to the relatively homogeneous water vapor content in the atmosphere [29]–[31]. Based on these properties of ZWD, it can be modeled as a random walk process and estimated in Kalman filtering by means of GNSS observations. However, it is inevitable that the pseudorange and carrier-phase observations are always contaminated by some level of receiver noise, since this noise is either generated by receiver electronics itself or caused by the connected antenna [32]. Besides, obstruction of tracking signals, large environment noise and interference signals may occur frequently, then lead to differing data quality and discontinuities of GNSS measurements even received by devices from the same manufacturer. As a result of the above facts, the accuracy as well as the precision of ZWD estimates is limited to some extent.

Considering the spatial resolution of atmospheric monitoring and the financial constraint of GNSS station construction, low-cost GNSS meteorology is necessary. Previous research [33] has demonstrated the feasibility and reliability of low-cost multi-GNSS receivers for meteorological applications. On the basis of that, this study is mainly concerned with multiple low-cost receiver sites, which are connected to a single antenna or are co-located over a horizontal distance of only a few meters separation. In order to provide a more precise and accurate common ZWD for these multi-receiver sites on a local scale and simultaneously estimate receiver coordinates, we propose a novel model by fusing GNSS measurements on the observation level. This fusion model utilizes the increased redundancy of raw observations from multiple sites to derive the combined ZWD estimates, which agree better with physical properties of the local wet refractivity field. In the following sections, we will first introduce the models involved in tropospheric estimation and the principle of the proposed model. Then a series of experiments are conducted to investigate the performance of the fusion model. The effectiveness and reliability of this approach are demonstrated by experimental analysis and results with respect to simulation and real data. In the last section, the conclusion and final remarks are given.

II. Method

A. Tropospheric delay models

The microwave signals experience propagation delays when passing through the neutral atmosphere (primarily the troposphere). This path delay is a major error source in the data analysis of the space geodetic techniques, like GNSS, Very Long Baseline Interferometry (VLBI) and Doppler orbitography and radiopositioning integrated by satellite (DORIS) [34]. Based on the assumption of the neutral atmosphere's azimuthal symmetry around the station, the troposphere path delay $\Delta L(e)$ at the elevation angle e is commonly represented in the form of [35]

$$\Delta L(e) = \mathrm{ZHD}\cdot mf_{\mathrm{h}}(e) + \mathrm{ZWD}\cdot mf_{\mathrm{w}}(e), \tag{1}$$

where the tropospheric delay modeling consists of two terms: the hydrostatic and the wet delay, referred to as ZHD and ZWD respectively. Each term is described as the product of the zenith delay and an elevation-dependent mapping function $mf(e)$.

According to the continued fraction form proposed by Marini (1972) [36] and normalized by Herring (1992) [37] for mapping the ZTD to the elevation of each observation, a variety of modern mapping functions exist. As one of most popular mapping functions in GNSS applications, the Vienna Mapping Functions 1 (VMF1, [38]) has been applied in this work. To provide the hydrostatic and wet VMF1 coefficients (a_{h} and a_{w}), the Global Pressure and Temperature 2 wet (GPT2w, [39]) is commonly utilized. It should be noted that when using the gridded VMF1, like VMF1 combined with GPT2w on a grid of $1^\circ\times1^\circ$, which is concerned in this study, the height correction of Niell (1996) [40] has to be additionally applied to the hydrostatic mapping function $mf_{\mathrm{h}}(e)$.

Alongside with being fully consistent with the coefficients a_{h} and a_{w} required for the computation of VMF1, GPT2w contains also a set of climatological parameters, such like the pressure p in hPa, that can be used as an input parameter together with the geographic latitude φ and ellipsoidal height h_{ell} of the site to calculate the ZHD by means of the Saastamoinen (1972) [41] model as refined by Davis et al. (1985) [35] as follows

$$\mathrm{ZHD} = 0.0022768\cdot\frac{p}{1-0.00266\cdot\cos(2\varphi)-0.28\cdot10^{-6}\cdot h_{\mathrm{ell}}}. \tag{2}$$

Whereas the ZWD is estimated as an unknown parameter in the Extended Kalman Filter (EKF) procedure (see the next subsection).

B. Uncombined PPP model and fusion model

In the uncombined PPP functional model, raw pseudorange (P) and carrier-phase (L) observations

$$\begin{aligned} P_{r,j}^{s} &= \rho_r^s + \mathrm{d}t_r - \mathrm{d}t^s + mf_r^s\cdot\mathrm{ZWD} \\ &\quad + \gamma_j\cdot I_r^s + B_{r,j} - B_j^s + \varepsilon_{r,j}^s \end{aligned} \tag{3}$$

$$\begin{aligned} L_{r,j}^{s} &= \rho_r^s + \mathrm{d}t_r - \mathrm{d}t^s + mf_r^s\cdot\mathrm{ZWD} \\ &\quad - \gamma_j\cdot I_r^s + \lambda_j\cdot\left(N_{r,j}^s + b_{r,j} - b_j^s\right) + \xi_{r,j}^s \end{aligned} \tag{4}$$

are used, where indices s, r identify the GNSS satellite and receiver; the subscript j refers to a given frequency band; ρ_r^s denotes the geometric distance between the satellite and receiver antenna phase centers, and with necessary corrections including slant hydrostatic delay, Sagnac effect, relativistic effects, tidal effects and phase wind-up (only for carrier-phases), which are assumed to be precisely modeled in advance; $\mathrm{d}t_r$ and $\mathrm{d}t^s$ are the receiver and satellite clock offsets, respectively; mf_r^s is the wet mapping function (i.e., wet VMF1 mapping function mf_{w} in this study); I_r^s is the slant ionospheric delay on the frequency f_1; $\gamma_j = f_1^2/f_j^2$ is a frequency-dependent ionospheric scaling factor; λ_j and $N_{r,j}$ are the carrier-phase

This article has been accepted for publication in IEEE Journal of Selected Topics in Applied Earth Observations and Remote Sensing. This is the author's version which has not been fully e
content may change prior to final publication. Citation information: DOI 10.1109/JSTARS.2024.3381792

wavelength and ambiguity on the frequency band j; $B_{r,j}$ and B_j^s denote the frequency-dependent uncalibrated code delay referring to receiver r and satellite s, respectively; $b_{r,j}$ and b_j^s stand the frequency-dependent receiver and satellite uncalibrated phase delays; $\varepsilon_{r,j}^s$ and $\xi_{r,j}^s$ are the sum of measurement noises and other unmodeled errors like multipath effects for pseudorange and carrier-phase observations.

After applying precise satellite orbit and clock products provided by the International GNSS Service (IGS) and reducing the effects of hydrostatic troposphere delay, the reduced observation equations in dual-frequency PPP can be written as follows [28], [42]

$$\begin{cases} P_{r,1}^s = \bar{\rho}_r^s + \mathrm{d}\bar{t}_r + mf_r^s \cdot \mathrm{ZWD} + \gamma_1 \cdot \bar{I}_r^s + \varepsilon_{r,1}^s \\ P_{r,2}^s = \bar{\rho}_r^s + \mathrm{d}\bar{t}_r + mf_r^s \cdot \mathrm{ZWD} + \gamma_2 \cdot \bar{I}_r^s + \varepsilon_{r,2}^s \\ L_{r,1}^s = \bar{\rho}_r^s + \mathrm{d}\bar{t}_r + mf_r^s \cdot \mathrm{ZWD} - \gamma_1 \cdot \bar{I}_r^s + \lambda_1 \cdot \bar{N}_{r,1}^s + \xi_{r,1}^s \\ L_{r,2}^s = \bar{\rho}_r^s + \mathrm{d}\bar{t}_r + mf_r^s \cdot \mathrm{ZWD} - \gamma_2 \cdot \bar{I}_r^s + \lambda_2 \cdot \bar{N}_{r,2}^s + \xi_{r,2}^s \end{cases} \tag{5}$$

with

$$\begin{cases} \mathrm{d}\bar{t}_r = \mathrm{d}t_r - \mathrm{d}_{r,\mathrm{IF}} \\ \bar{I}_r^s = I_r^s - \beta_{12} \cdot (\mathrm{DCB}_{r,12} - \mathrm{DCB}_{12}^s) \\ \bar{N}_{r,1}^s = N_{r,1}^s + b_{r,1} - b_1^s + (\mathrm{d}_{r,\mathrm{IF}} - \mathrm{d}_{\mathrm{IF}}^s)/\lambda_1 \\ \qquad - \gamma_1 \cdot \beta_{12} \cdot (\mathrm{DCB}_{r,12} - \mathrm{DCB}_{12}^s)/\lambda_1 \\ \bar{N}_{r,2}^s = N_{r,2}^s + b_{r,2} - b_2^s + (\mathrm{d}_{r,\mathrm{IF}} - \mathrm{d}_{\mathrm{IF}}^s)/\lambda_2 \\ \qquad - \gamma_2 \cdot \beta_{12} \cdot (\mathrm{DCB}_{r,12} - \mathrm{DCB}_{12}^s)/\lambda_2 \end{cases} \tag{6}$$

$$\begin{cases} \alpha_{12} = f_1^2 / \left(f_1^2 - f_2^2\right), \ \beta_{12} = 1 - \alpha_{12} = -f_2^2 / \left(f_1^2 - f_2^2\right) \\ d_{r,\mathrm{IF}} = \alpha_{12} \cdot B_{r,1} + \beta_{12} \cdot B_{r,2}, \ d_{\mathrm{IF}}^s = \alpha_{12} \cdot B_1^s + \beta_{12} \cdot B_2^s \\ \mathrm{DCB}_{r,12} = B_{r,1} - B_{r,2}, \ \mathrm{DCB}_{12}^s = B_1^s - B_2^s \end{cases} \tag{7}$$

therein $\bar{\rho}_r^s$ denotes the geometric distance in the use of IGS precision products to fix the satellite orbit and clock offset; $d_{r,\mathrm{IF}}$ and d_{IF}^s are the ionosphere-free (IF) pseudorange hardware delay at the receiver r and the satellite s, respectively; $\mathrm{DCB}_{r,12}$ and DCB_{12}^s represent the receiver and satellite differential code bias (DCB) between pseudorange $P_{r,1}^s$ and $P_{r,2}^s$. In the standard dual-frequency PPP model, hardware biases are normally not estimated. According to equation (6), hardware delay biases from pseudoranges can be absorbed by both receiver clock offset and slant ionospheric delay parameters, while ambiguity parameters absorb receiver and satellite hardware delays from both pseudorange and carrier-phase observations, thus losing the integer property [27]. Hence, parameters to be estimated include receiver position coordinates $(x, y, z)^T$, the receiver clock parameter $\mathrm{d}\bar{t}_r$, the ZWD, slant ionospheric delays $\bar{I}_r^s$ as well as float carrier-phase ambiguities on both frequency bands $\bar{N}_{r,1}^s$ and $\bar{N}_{r,2}^s$. In addition, to process the GNSS data from multi-constellations, the inter-system bias (ISB) is introduced, that takes not only the receiver-dependent IF pseudorange hardware delay differences between different GNSS constellations (e.g., GPS and Galieo), i.e., $(d_{r,\mathrm{IF}})^{\mathrm{GPS}} - (d_{r,\mathrm{IF}})^{\mathrm{Galileo}}$ into account, but also the receiver-independent time differences generated by different clock datum constraints from external GNSS satellite clock products [43]. Therefore, the estimation of ISBs is more preferable than the individual estimation of receiver clock offsets for each satellite system.

This study is based on the dual-frequency PPP for which parameter are estimated by the help of an EKF, in which the state vector $\boldsymbol{x}_k$ at epoch k can be expressed as

$$\boldsymbol{x}_k = \left[\underbrace{x, y, z}_{\text{pos}} \middle| \underbrace{\mathrm{d}\bar{t}_r, \mathrm{ISB}_r^s}_{\text{clk}} \middle| \mathrm{ZWD} \middle| \underbrace{\bar{I}_r^s}_{\text{ion}} \middle| \underbrace{\bar{N}_{r,1}^s, \bar{N}_{r,2}^s}_{\text{amb}} \right]^T. \tag{8}$$

Due to the temporal behavior, all the estimated parameters are commonly assumed as random-walk processes, the discrete formulation of the state vector is then given by

$$\boldsymbol{x}_k = \boldsymbol{\Phi}_{k|k-1} \boldsymbol{x}_{k-1} + \boldsymbol{u}_k, \tag{9}$$

where $\boldsymbol{\Phi}_{k|k-1}$ denotes the state transition matrix, which is set to an identity matrix in the random walk model; $\boldsymbol{u}_k$ is the random error vector including Gaussian white noises of all estimated states as follows

$$\boldsymbol{u}_k = [u_{\mathrm{pos}}, u_{\mathrm{clk}}, u_{\mathrm{ZWD}}, u_{\mathrm{ion}}, u_{\mathrm{amb}}]^T \tag{10}$$

$$\boldsymbol{E}\left\{\boldsymbol{u}_k \boldsymbol{u}_n^T\right\} = \begin{cases} \boldsymbol{Q}_k, & n = k \\ \boldsymbol{0}, & n \neq k \end{cases} \tag{11}$$
$$\text{with} \quad \boldsymbol{Q}_k = \mathrm{diag}\left(\sigma_{\mathrm{pos}}^2, \sigma_{\mathrm{clk}}^2, \sigma_{\mathrm{ZWD}}^2, \sigma_{\mathrm{ion}}^2, \sigma_{\mathrm{amb}}^2\right) \cdot \Delta t$$

where $\boldsymbol{E}\{\cdot\}$ denotes the expectation operation; $\boldsymbol{Q}_k$ represents the process noise Variance-Covariance (VC) matrix, which is defined by the noise spectral density σ^2 of all states. In this work, the spectral density value for the ZWD parameter is empirically set to $(4\,\mathrm{mm}/\sqrt{\mathrm{h}})^2/\mathrm{s}$ [7]. The stochastic models in Kalman filtering are built under the assumption that either the process noise or the measurement noise follows a zero-mean Gaussian distribution, and both noises are mutually uncorrelated. On basis of this, the EKF is processed by a "predict-update" loop, its formulation is summarized as [44]

Prediction:

$$\hat{\boldsymbol{x}}_{k|k-1} = \boldsymbol{\Phi}_{k|k-1} \hat{\boldsymbol{x}}_{k-1|k-1} \tag{12}$$
$$\boldsymbol{P}_{k|k-1} = \boldsymbol{\Phi}_{k|k-1} \boldsymbol{P}_{k-1|k-1} \boldsymbol{\Phi}_{k|k-1}^T + \boldsymbol{Q}_k \tag{13}$$

Updating:

$$\boldsymbol{K}_k = \boldsymbol{P}_{k|k-1} \boldsymbol{H}_k^T \left[\boldsymbol{H}_k \boldsymbol{P}_{k|k-1} \boldsymbol{H}_k^T + \boldsymbol{R}_k\right]^{-1} \tag{14}$$
$$\hat{\boldsymbol{x}}_{k|k} = \hat{\boldsymbol{x}}_{k|k-1} + \boldsymbol{K}_k \left(\boldsymbol{z}_k - \boldsymbol{H}_k \hat{\boldsymbol{x}}_{k|k-1}\right) \tag{15}$$
$$\boldsymbol{P}_{k|k} = \left(\boldsymbol{I} - \boldsymbol{K}_k \boldsymbol{H}_k\right) \boldsymbol{P}_{k|k-1} \tag{16}$$

where the superscript k indicates the k-th epoch; $\hat{\boldsymbol{x}}_{k|k-1}$ and $\boldsymbol{P}_{k|k-1}$ denote the predicted state vector and its VC matrix; $\hat{\boldsymbol{x}}_{k|k}$ is the updated state vector, $\boldsymbol{P}_{k|k}$ is its corresponding VC matrix; $\boldsymbol{K}_k$ represents the Kalman gain; $\boldsymbol{z}_k$ is the measurement vector; $\boldsymbol{H}_k$ denotes the design matrix describing the correlation between measurements and the states; $\boldsymbol{R}_k$ is the measurement noise VC matrix, which is a diagonal matrix as well as $\boldsymbol{Q}_k$. Accouting that low-elevation observations are more prone to effects of GNSS signal refraction and reflection, the elevation-dependent weighting of observations is generally applied to improve the estimation accuracy. Herein, the

This article has been accepted for publication in IEEE Journal of Selected Topics in Applied Earth Observations and Remote Sensing. This is the author's version which has not been fully edited and
content may change prior to final publication. Citation information: DOI 10.1109/JSTARS.2024.3381792

stochastic model of undifferenced observations is defined as a sine function

$$\sigma_{\text{obs}}^2 = \frac{a^2}{\sin^2(e)}, \tag{17}$$

where σ_{obs}^2 is the variance of the measurement noise; e is the satellite elevation angle; a is the empirical coefficient referring to the C/A code and P(Y) code pseudorange and carrier-phase measurement, which is chosen as 0.9 m, 0.3 m and $(0.01/9)$ m, respectively, as the noise of pseudorange measurements is approximately 100 times greater than that of carrier-phase measurements. In addition, the elevation cut-off angle is set to $5°$ in all conducted experiments.

It should be noted that unlike the well-deterministic state-space function model, the stochastic model is usually approximated due to the lack of complete knowledge about noise characteristics and the numerical computation strategy [45]. The estimation procedure in this work is constructed with the assumption of white Gaussian noises for the optimal Kalman filter without considering any time-correlation. However, colored and correlated system noises are likely to be present in practice, which requires a more realistic stochastic model and thus are subject further study.

The proposed fusion model aims to estimate one common ZWD parameter with less noise for multiple receiver sites mounted in a limited or small region, its state vector $\boldsymbol{x}_k$ for several receiver sites with the number of i is defined as follows

$$\boldsymbol{x}_k = \Big[\text{ZWD} \;\Big|\; \underbrace{x_1, y_1, z_1}_{\text{pos}_1} \;\Big|\; \underbrace{\text{d}\bar{t}_{r_1}, \text{ISB}_{r_1}^s}_{\text{clk}_1} \;\Big|\; \underbrace{\bar{I}_{r_1}^s}_{\text{ion}_1} \;\Big|\; \underbrace{\bar{N}_{r_1,1}^s, \bar{N}_{r_1,2}^s}_{\text{amb}_1} \;\Big| \\ \cdots \;\Big|\; \underbrace{x_i, y_i, z_i}_{\text{pos}_i} \;\Big|\; \underbrace{\text{d}\bar{t}_{r_i}, \text{ISB}_{r_i}^s}_{\text{clk}_i} \;\Big|\; \underbrace{\bar{I}_{r_i}^s}_{\text{ion}_i} \;\Big|\; \underbrace{\bar{N}_{r_i,1}^s, \bar{N}_{r_i,2}^s}_{\text{amb}_i} \Big]^T. \tag{18}$$

The corresponding state VC matrix $\boldsymbol{P}_k$ contains the correlation among all the estimated parameters, its diagonal entries reveal the estimation precision of Kalman filtering. Figure 1 illustrates the EKF procedure either for the undifferenced PPP model or for the proposed fusion model.

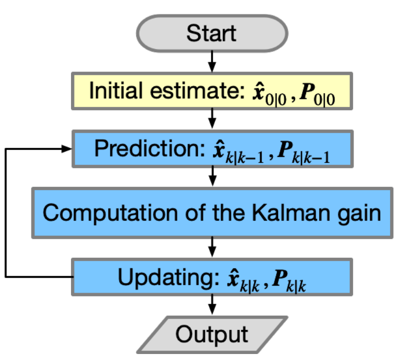

Fig. 1: Overview of the EKF process

III. Experiments

A. GNSS data and processing strategy

To evaluate the performance of the fusion model, simulated and realistic experiments are conducted. In the following experimental results and analysis, GPS and Galileo pseudorange and carrier-phase measurements on frequencies L1, L2, E1 and E5b are processed with data intervals of 30 seconds in three scenarios:

Scenario 1: Software-in-the-loop (SIL) simulation with a commercial GNSS simulator, hereafter this scenario is referred to as simulation-virtual mode

Scenario 2: Hardware-in-the-loop (HIL) simulation with a commercial GNSS simulator, hereafter this scenario is referred to as simulation-hardware mode

Scenario 3: Data from a field campaign - hereafter referred to as low-cost demonstration test

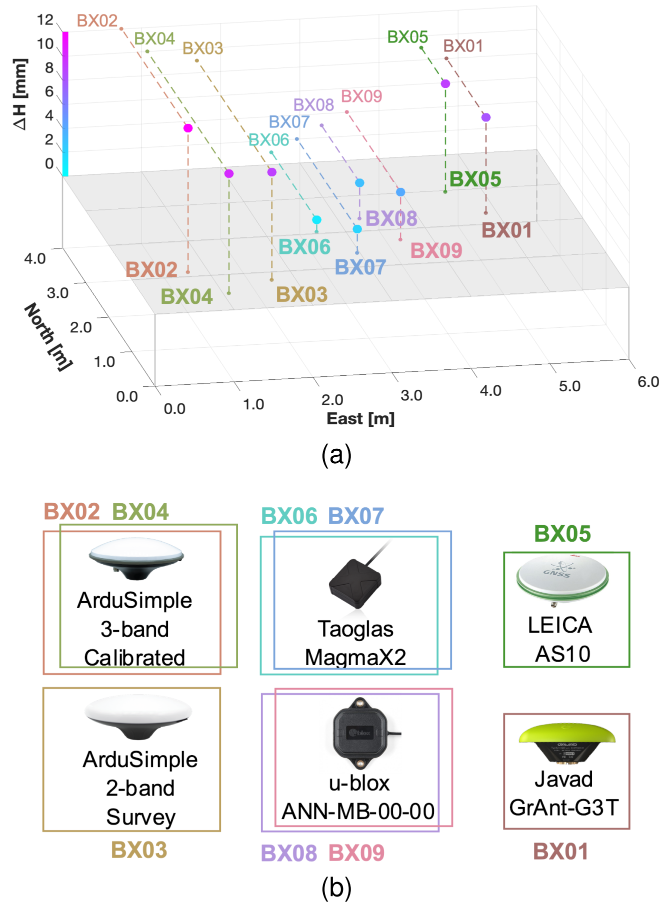

Fig. 2: Experimental setup. (a) Locations of nine "BX"-sites with the height difference. (b) Concept of the connection between the GNSS receiver and antenna, as well as the antenna type.

The real data applied in the low-cost demonstration test was collected for nine sites from 5 to 17 July 2022, with a sampling rate of 30 seconds. These nine sites are located on the roof of the Institute of Geodesy and Geoinformatics (IGG) at the Wrocław University of Environmental and Life Sciences in Poland, and equipped with multiple u-blox ZED-F9P receivers connected to rooftop GNSS antennas on a platform. As shown in figure 2, each low-cost receiver is connected to either a single antenna or antennas which are separated horizontally by only a few meters. The field setup is based on short baselines and with height differences of less than 12 mm, which are derived from reference coordinates determined by means of

GNSS, leveling and tachymetry. In the observation model, the satellite antenna corrections have been considered using the Antenna Exchange format (ANTEX) file igsR3_2077.atx, however, Phase Center Offsets (PCOs) and Phase Center Variations (PCVs) of most applied receiver antennas cannot be corrected due to unavailable calibration information for low-cost antennas like the u-blox ANN-MB antenna, the Taoglas MagmaX2 antenna, etc. Such uncorrected PCO/PCVs will bias the estimated position, especially in the height, as well as tropospheric estimates to some extent. Therefore, we also performed relevant simulations to better analyze the accuracy in position and ZTD estimation.

The simulation tests (scenarios 1 and 2) are conducted by using our Spirent GNSS simulator, which is able to generate pseudorange and carrier-phase observations based on the user-defined station coordinates and observation time. In addition, the generated GNSS signals can be transmitted to an external GNSS receiver on demand. Accounting for the effect of receiver noises, we perform the simulation with two modes: virtual mode and hardware mode, representing the application of GNSS simulator without and with the connection to the u-blox ZED-F9P receiver, respectively. In both modes, atmospheric effects are not simulated, that is, the reference ZWD or ZTD is exactly zero. This allows us to evaluate precision and accuracy of the estimates, which is usually not possible since no absolute ground-truth is available for judging the accuracy of meteorologic parameters. Besides, to preserve the actual noise characteristics of the GNSS observations in the virtual mode, we artificially introduce normally distributed noises with zero-mean and standard deviation of 50 cm and 5 mm to pseudoranges and carrier-phases, respectively. During the simulation, the virtual mode with nine virtual receivers corresponds to the experiment in practice, its observation period keeps the same as the real data, and the reference coordinates illustrated in figure 2 are provided as inputs to the GNSS Simulator. Differing from that, the hardware mode is performed at one common static site for 48 hours by using the same u-blox ZED-F9P receiver, and the simulated data with the same period is repeatedly received for nine times.

To evaluate the accuracy of tropospheric estimates, two data sources are used as a reference, i.e., the NRT ZTD estimate, and the microwave radiometer, both at 15-minute intervals. The NRT ZTD product for the WROC station is provided by IGG for the E-GVAP programme with an estimated uncertainty of 0.7 to 2.8 mm. The RPG-HATPRO-G5 (Humidity And Temperature PROfiler, single-polarization) microwave radiometer is co-located with the WROC station. The standard deviation of ZTD differences between the radiometer ZTD and the radiosonde ZTD is 7.4 mm [46]. Based on undifferenced GNSS measurements from simulated and realistic experiments, the uncombined PPP model and fusion model are separately performed for each dataset. In the evaluation of the ZTD error, statistical results including the standard deviation (STD), mean absolute error (MAE) and root-mean-square (RMS) error are provided. Besides, we utilize the software "Stable32" [47] to compute the overlapping Allan deviation (ADEV) of ZTD estimates, so that the corresponding noise level can be investigated. In this study, we focus only on the solution after the Kalman filter converges, i.e., after 6 hours for all datasets, the convergence time is not concerned and discussed.

B. Datasets assessment

1) **ZWD precision and accuracy:** We first evaluate the ZWD estimation in the fusion model compared to the PPP model, as displayed in figure 3. For either mode, the blue combined ZWD from the fusion model exhibit less jumps with respect to ZWD estimates in the PPP model represented by other colours. In both simulations, the estimated ZWD varies by no more than 10 mm, which is close to the near-zero reference value. Since the simulation-virtual mode without the connection to the low-cost receiver, ZWD estimates from both models show more homogenous and are better to agree with the white noise feature. The right panel of figure 3 illustrates the formal error of the ZWD estimation, which is derived from the state VC matrix and indicates the precision of Kalman filtering. In comparison to PPP results, which have mean values ranging from 0.73 to 0.80 mm, the formal error in ZWD estimation based on the fusion approach can always reach the lowest with the mean value of 0.35 mm, 0.37 mm and 0.35 mm for three scenarios, respectively.

TABLE I: Statistics analysis of the ZTD error with the simulated dataset

simulation-virtual mode

Virtual sites	STD [mm]	MAE [mm]	RMS [mm]
BX01	1.58	1.24	1.58
BX02	1.51	1.19	1.51
BX03	1.58	1.23	1.58
BX04	1.56	1.21	1.56
BX05	1.59	1.25	1.60
BX06	1.59	1.24	1.59
BX07	1.59	1.25	1.60
BX08	1.59	1.24	1.59
BX09	1.55	1.21	1.55
Fusion	**1.10**	**0.85**	**1.10**

simulation-hardware mode

Virtual sites	STD [mm]	MAE [mm]	RMS [mm]
REC1	0.45	0.35	0.45
REC2	0.43	0.34	0.43
REC3	0.44	0.35	0.46
REC4	0.54	0.36	0.54
REC5	0.45	0.38	0.48
REC6	0.42	0.32	0.42
REC7	0.53	0.41	0.57
REC8	0.41	0.33	0.41
REC9	0.42	0.33	0.43
Fusion	**0.29**	**0.23**	**0.30**

To quantitatively analyze the ZTD accuracy, which enable to reflect the accuracy in ZWD estimation, we compute the STD, MAE and RMS of differences between ZTD estimates and their reference values using all three datasets, as listed in Table I and II. In the simulation, the corresponding STD, MAE and RMS of ZTD errors are consistent with those of ZWD errors as the atmospheric effect is not simulated. When estimating ZTD time series in practice, the reference source

This article has been accepted for publication in IEEE Journal of Selected Topics in Applied Earth Observations and Remote Sensing. This is the author's version which has not been fully e
content may change prior to final publication. Citation information: DOI 10.1109/JSTARS.2024.3381792

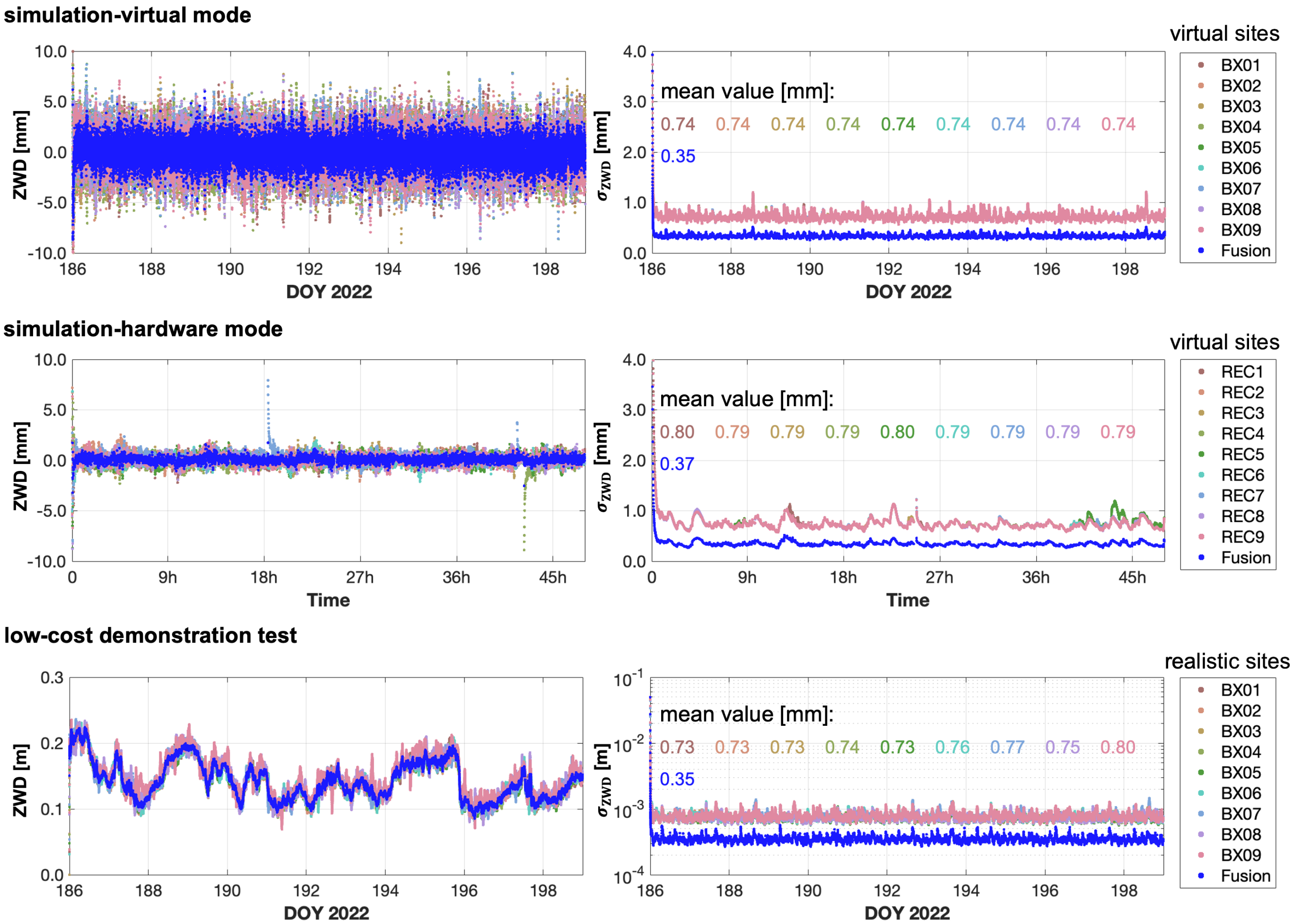

Fig. 3: ZWD estimates and their formal errors from the simulation-virtual mode (top panel), the simulation-hardware mode (middle panel) and the low-cost demonstration test (bottom panel). Left plots depict the estimated ZWD states, whereas the right plots show the corresponding formal error of the filter state.

TABLE II: Statistics analysis of the ZTD error with the real dataset

low-cost demonstration test

Realistic sites	STD [mm] Radiometer	STD [mm] NRT	MAE [mm] Radiometer	MAE [mm] NRT	RMS [mm] Radiometer	RMS [mm] NRT
BX01	10.13	8.39	6.70	6.76	10.18	8.97
BX02	9.19	7.28	6.47	5.84	10.15	7.57
BX03	9.20	7.49	5.57	5.88	9.24	7.62
BX04	9.40	7.53	5.93	5.80	9.47	7.61
BX05	9.17	7.17	6.00	5.52	9.59	7.19
BX06	10.06	8.66	6.97	7.15	10.10	9.21
BX07	10.33	9.00	7.06	7.37	10.40	9.66
BX08	12.54	10.72	10.06	10.28	13.36	12.73
BX09	14.13	12.16	12.16	12.49	15.95	15.52
Fusion	**9.05**	**6.97**	**5.56**	**5.67**	**9.05**	**7.43**

data with the time interval of 15 minutes come from the NRT ZTD values and the radiometer. Either for whichever dataset or mode with/without the connection to the low-cost receiver, or these multiple sites are separately located in a limited region, or they are colocated, the STDs of ZTD errors in the fusion model have the lowest value compared to ones in the PPP model. In addition, apart from the case using the real data that BX05's MAE and RMS with respect to the reference ZTD from the radiometer are lower in the PPP model than in the fusion model, other MAEs and RMSs of ZTD errors derived from the combined ZWD are superior to single receiver estimates for each station. The reason for that could be the geodetic-grade Leica AS10 GNSS antenna mounted at the receiver site BX05 is the only one with the available PCO/PCV calibration information, and the related corrections are applied in the data-processing. In such case, the combined ZWD by fusing GNSS measurements based on the observation level may be degraded to some extent due to the most receiver antennas, which lack phase center corrections. Despite this, the fusion model has a more reliable and accurate performance for the tropospheric estimation, especially for four receiver sites BX06, BX07, BX08 and BX09 using low-cost patch antennas, where the RMS of ZTD errors based on the fusion approach can be reduced by the range of 1 to 7 mm and 2 to 8 mm with respect to radiometer values and NRT ZTDs, respectively. The improvement for the STD of differences between the estimated ZTD and reference radiometer data as well as NRT ZTDs can range from 1 to 5 mm, from 2 to 6 mm, respectively; for the

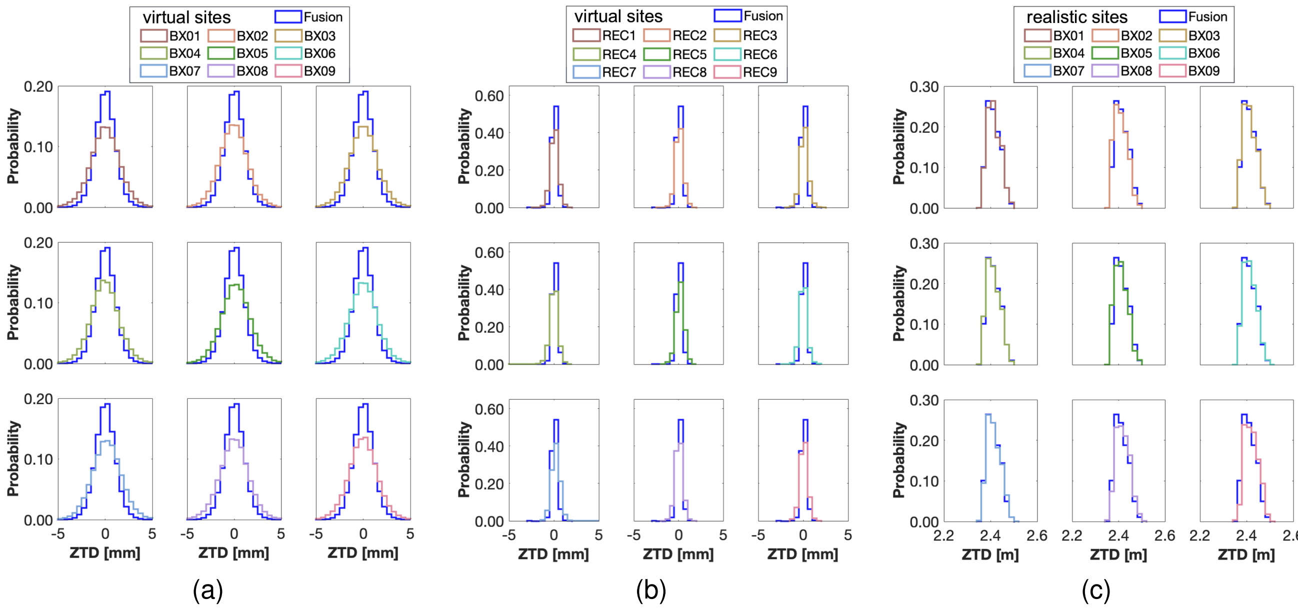

Fig. 4: Probability distribution histogram of ZTD estimates. (a) simulation-virtual mode. (b) simulation-hardware mode. (c) low-cost demonstration test.

MAE of those from 1 to 7 mm and 2 to 7 mm.

Figure 4 depicts the probability distribution histogram of ZTD time series. In the typical application, the ZWD parameter is estimated as a random walk process. If there are no unmodeled error or all the noise involved is white, the tropospheric estimation either for ZWD or ZTD is expected to follow a Gaussian distribution and with a similar probability distribution histogram as displayed in figure 4a. Due to the low-cost receiver containing random noises for each measurement at each simulation round, the estimated ZWDs in the PPP model are different in the simulation-hardware mode, even when using the same receiver at one common location. This results in a change in the probability distribution of ZTD estimates. Generally, the ZHD calculated by the Saastamoinen model is less variable on small areas, the variation of ZTD estimation is mainly influenced by the ZWD estimation due to the rapid change of water vapor. Without any atmospheric and multipath effects during the simulation, the ZTD from the fusion model is more likely to be distributed at the near-zero reference. Though there are many factors in practice, such as signal refraction and reflection, that could interfere with measurements and potentially create more noises which differ from the white noise and are not appropriately modeled, the probability distribution of ZTD estimates in the fusion model is relatively more concentrated than those in the PPP model for most sites, especially for BX08 and BX09. In general one would expect, that systematic effects, like e.g. multi-path, are affecting all receivers at the same level since they are placed relatively close to each other or are even connected to the same antenna. Thus, the major improvement from the fusion approach is thought to emerge from the fact that white noise processes are uncorrelated across different receivers and thus lead to a significant reduction in random errors of the fused ZWD estimates.

2) **ZTD stability:** The stability analysis of ZTD time series is conducted using the overlapping ADEV, which is a commonly used measure of frequency stability. Figure 5 depicts the sigma-tau diagram for each mode, which reflects the dependence of stability on averaging time. It can be determined that the longer the observation time, the more random processes are averaged out, leading to a decrease in variability and an improvement in stability. In both simulation modes where ZTD and ZWD are not numerically different, the fusion curves consistently show lower values compared to the other curves of the PPP model as the averaging time τ increases. This suggests that the fusion approach provides a more stable and less noisy estimation of ZWD. The realistic experiment depicted in figure 5c also demonstrates that the fusion curve has relatively less noise and a steeper slope compared to the other PPP curves, similar to the simulation results. Additionally, it can be observed that the overlapping ADEV of ZTD computed by means of the reference data from the radiometer and NRT ZTDs have a different starting point than the one based on GNSS measurements. This difference arises from the fact that the radiometer and NRT ZTDs have a 15-minute sampling rate (900 seconds), while GNSS measurements have a sampling rate of 30 seconds. Nevertheless, as more random processes are averaged, the fusion curve gradually converges towards the reference curve of NRT ZTDs, and both are more stable than the radiometer curve.

3) **Coordinate domain:** To further assess the benefit of the fusion approach in terms of positioning accuracy, we concentrate solely on experiments conducted using simulated data with known reference coordinates rather than the real dataset, as most receiver sites lack the antenna phase center

This article has been accepted for publication in IEEE Journal of Selected Topics in Applied Earth Observations and Remote Sensing. This is the author's version which has not been fully e
content may change prior to final publication. Citation information: DOI 10.1109/JSTARS.2024.3381792

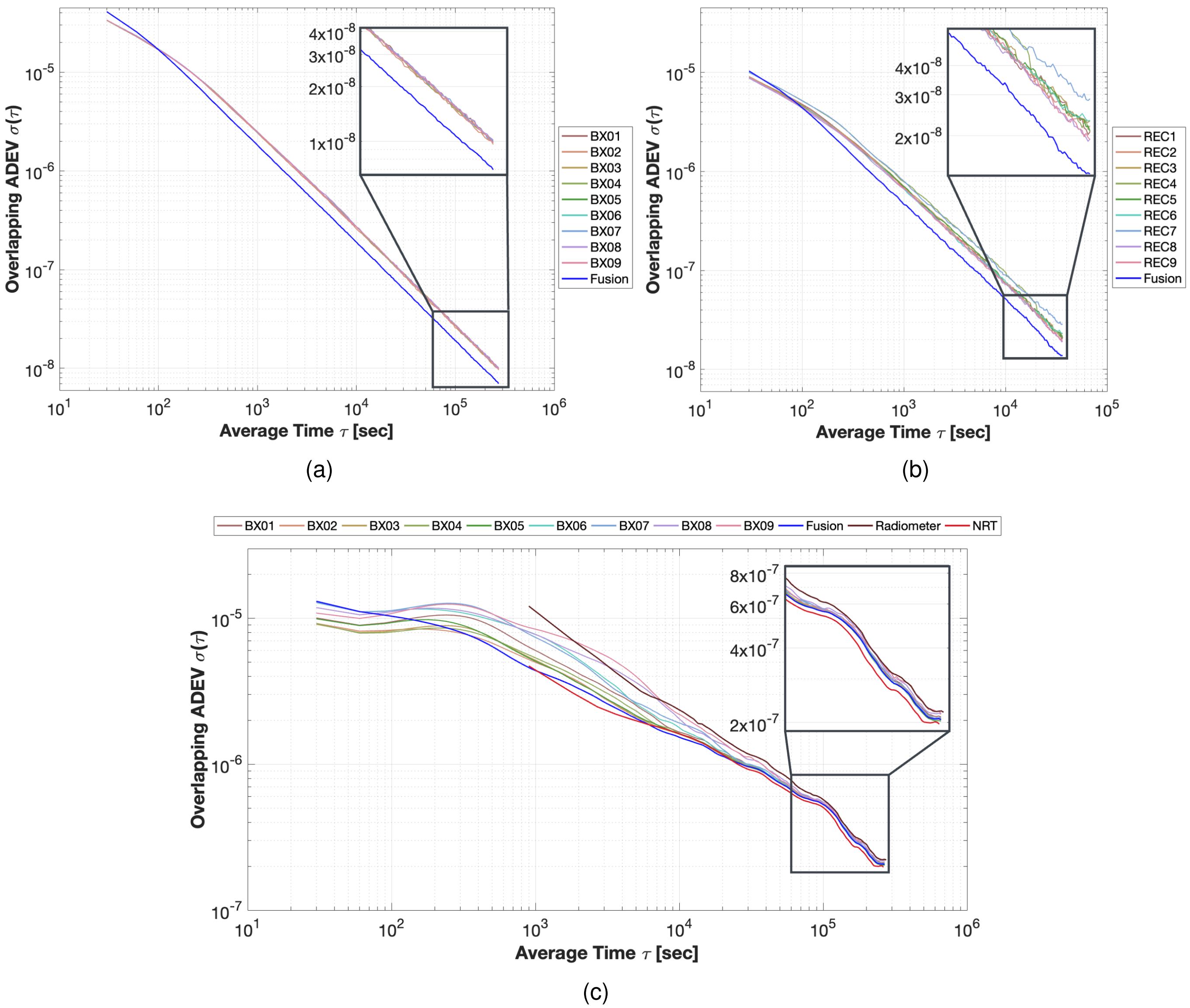

Fig. 5: Overlapping ADEV of ZTD estimates. (a) simulation-virtual mode for 13 days. (b) simulation-hardware mode for 48 h. (c) low-cost demonstration test for 13 days with respect to reference values from the radiometer and NRT ZTDs.

correction, resulting in a compromised position estimation. Figure 6 displays the RMS of the positioning error in east, north, and up components after filter convergence for both simulation modes. Overall, most horizontal components of the two models exhibit minimal differences, with variations of less than 0.05 mm, whereas the improvement in the upward component is notable when applying the one common ZWD to estimate the receiver coordinates for each sites in the fusion model. The vertical accuracy can be increased by a maximum of 48% and 47% for the mode with and without the connection to the low-cost receiver, respectively. Compared to the PPP model, RMS values of positional estimates, i.e., positioning 3D errors, can also achieve a significant improvement using the fusion approach, as depicted in figure 7. While all nine sites are able to enhance positioning accuracy with a maximal improvement of 24% in the simulation-virtual mode based on the fusion model, the site 3 which is connected to the low-cost receiver experiences a degradation of 0.1 mm due to a relatively large bias of approximately 0.2 mm in the east component. Despite this, the fused solution can provide a maximum 37% improvement in position estimation accuracy for the other receivers.

IV. Conclusions

To enhance the precision and accuracy of ZWD estimates in GNSS meteorology, this work presents a novel fusion model to obtain a common ZWD for multiple receiver sites in a dense GNSS antenna array on a limited scale. In tropospheric modeling, the VMF1 combined with the GPT2w model is applied to precisely characterize the spatial and temporal variation of the atmosphere. The ZHD with less variability is obtained by the Saastamoinen model, whereas the ZWD is

This article has been accepted for publication in IEEE Journal of Selected Topics in Applied Earth Observations and Remote Sensing. This is the author's version which has not been fully e
content may change prior to final publication. Citation information: DOI 10.1109/JSTARS.2024.3381792

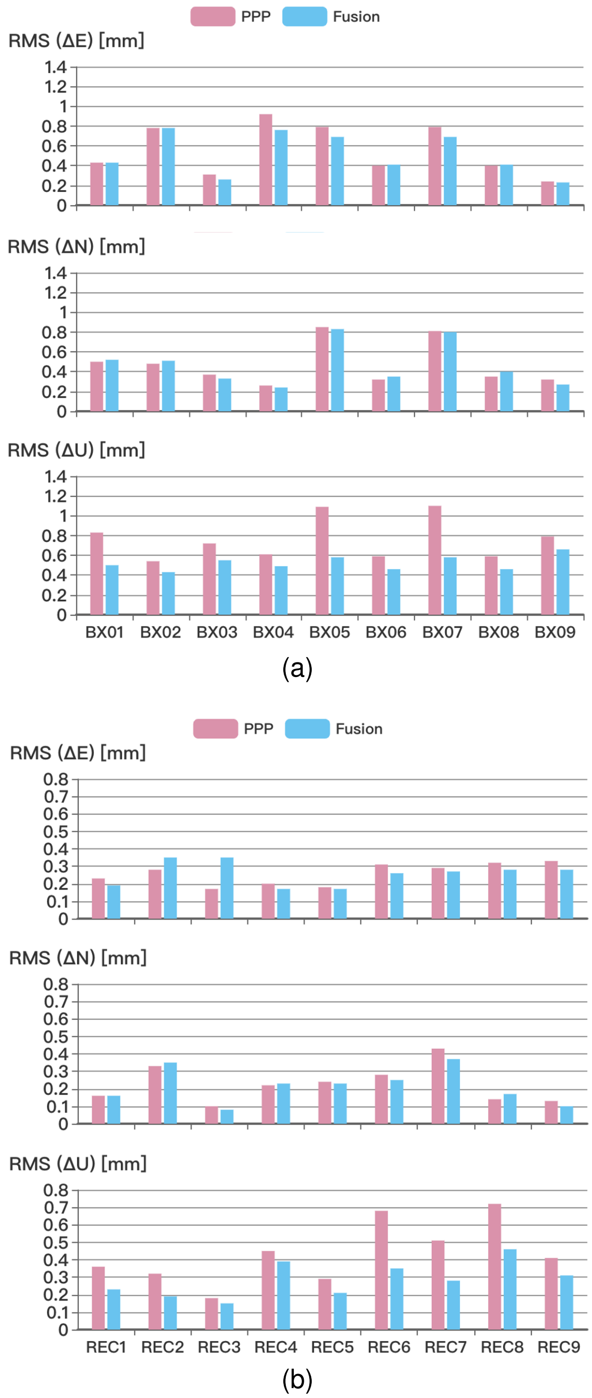

Fig. 6: RMS values of position estimation errors in east, north and up components. (a) simulation-virtual mode. (b) simulation-hardware mode.

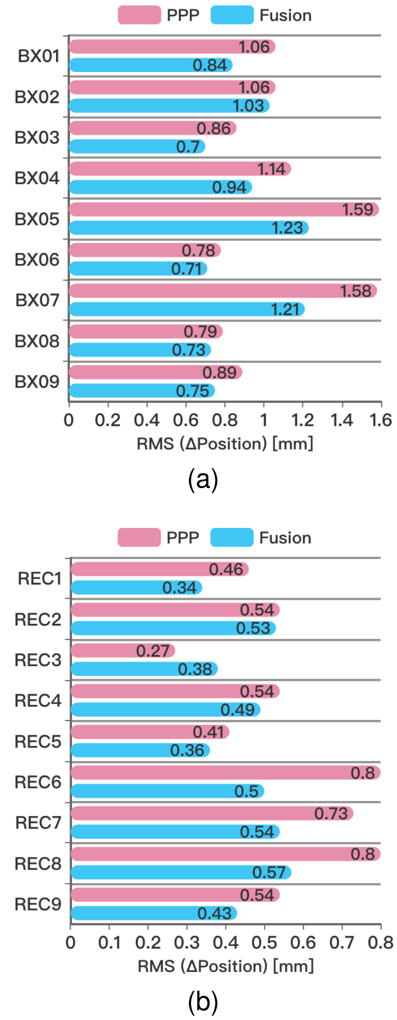

Fig. 7: 3D RMS errors in the positioning estimation. (a) simulation-virtual mode. (b) simulation-hardware mode.

estimated together with other unknown parameters due to the highly spatio-temporal change of water vapor. Therefore, the variation of derived ZTD is mainly dependent on the ZWD estimates.

According to ZWD time series and their formal error by means of the simulated and real dataset, it is demonstrated that these common ZWD estimates are superior to single receiver estimates in terms of precision. Compared to single receiver PPP results, the fusion results reveal a better accuracy with the lowest statistic values in both simulation experiments. In the practical experiment with 9 receivers, STD values for all receiver sites are improved, and with a maximal improvement of 36% and 43% with respect to the reference radiometer data and NRT ZTDs, respectively, as well as RMS and MAE values by using the radiometer as reference, which exhibit a higher accuracy increased by a maximum of 43% and 54%, respectively. It should be noted that the antenna phase center correction is not processed at most receiver sites due to the lack of available calibration information, which is also a limitation by using low-cost GNSS antennas, and consequently compromises the estimation of position, especially for the upward components, as well as the tropospheric estimation to some extent. Despite this, the fusion approach can present a notable improvement in RMS and MAE values of ZTD errors with respect to reference NRT ZTDs for most receiver sites. Besides, in analysis of the probability distribution of ZTD estimates, it can be observed that ZTD estimates in fusion model is more likely to be concentratively distributed than those in the PPP model for most sites, which is consistent with the quantitative assessment of the ZTD accuracy.

In low-cost GNSS meteorology applications, tropospheric estimation is prone to be limited especially due to the receiver noise. To demonstrate the high stability and noise resistance of these combined ZWD estimates by fusing data from multiple low-cost receivers, the overlapping ADEV of ZTD estimates is applied. Either in the simulated or realistic experiments, the fusion curve has less noise than the other PPP curves. In addition, as the observation time increases, the fusion curve is more comparable to the reference curve of NRT ZTDs, and both experience more significant stability than the radiometer curve. Furthermore, the advantage of the fusion concept in terms of positioning accuracy is confirmed by RMS errors of positioning estimation in east, north and up components and of the 3D positional estimates based on the simulated dataset. In summary, the accuracy in the upward component is increased by a maximum of 48% and 47%, resulting in the 3D RMS error can also be improved by a maximum of 37% and 24%, in the scenario with and without the connection to the low-cost receiver, respectively. However, horizontal components cannot benefit significantly from the combined ZWD. In this regard, effective outlier detection and further research are required.

It can be concluded that the proposed fusion model outperforms the undifferentiated PPP model in terms of precision, accuracy and noise level in tropospheric estimation. That enables the application of low-cost GNSS receivers for GNSS meteorology more accurate and reliable, making it possible to extend the application of this fusion approach from the local scale to regional and to benefit more GNSS positioning activities. Moreover, the clear benefit for positioning applications, in particular for the vertical coordinate components, motivates the fusion of two or more low-lost receivers which are connected to the same antenna. Thus such a very affordable set-up has the potential to compete with expensive geodetic-grade receivers, while also being able to improve robustness, availability and integrity. Therefore, more practical situations should be addressed in the future.

ACKNOWLEDGMENT

This study is related to the project "Simultaneous Troposphere Estimation with Precise Point Positioning (STEPPP)". Rui Wang is supported by the German Research Foundation (DFG, project number HO 5877/1-1). Grzegorz Marut is supported by the National Science Centre, Poland (NCN), Grant No. 2020/39/I/ST10/01318. The authors acknowledge colleagues who provide the noise generator in the simulation data processing.

AUTHOR CONTRIBUTIONS

Rui Wang participated in discussions related to the research's theoretical framework, completed in the development of the algorithm, performed simulation experiments, contributed to data analysis, provided result visualization, and drafted the initial manuscript; Grzegorz Marut provided a low-cost GNSS receiver for the simulation-hardware mode, designed and performed the field test campaign, and preprocessed low-cost GNSS data; Tomasz Hadas co-designed the experiment, validated the implementation of the algorithm, and supervised Grzegorz Marut; Thomas Hobiger co-designed the experiment and supervised Rui Wang. All authors provided critical feedback and contributed to the writing of the manuscript. All authors approved the submitted version of this manuscript.

DECLARATION OF INTERESTS

The authors declare no competing interests.

REFERENCES

[1] F. Zhang, J.-P. Barriot, G. Xu, and M. Hopuare, "Modeling the Slant Wet Delays From One GPS Receiver as a Series Expansion With Respect to Time and Space: Theory and an Example of Application for the Tahiti Island," *IEEE Transactions on Geoscience and Remote Sensing*, vol. 58, no. 11, pp. 7520–7532, 2020.

[2] H. Janes, R. Langley, and S. Newby, "Analysis of tropospheric delay prediction models: comparisons with ray-tracing and implications for GPS relative positioning," *Bulletin géodésique*, vol. 65, pp. 151–161, 1991.

[3] J. Boehm, B. Werl, and H. Schuh, "Troposphere mapping functions for GPS and very long baseline interferometry from European Centre for Medium-Range Weather Forecasts operational analysis data," *Journal of geophysical research: solid earth*, vol. 111, no. B2, 2006.

[4] A. Klos, J. Bogusz, R. Pacione, V. Humphrey, and H. Dobslaw, "Investigating temporal and spatial patterns in the stochastic component of ZTD time series over Europe," *GPS Solutions*, vol. 27, no. 1, p. 19, 2023.

[5] S. Jin, J.-U. Park, J.-H. Cho, and P.-H. Park, "Seasonal variability of GPS-derived zenith tropospheric delay (1994–2006) and climate implications," *Journal of geophysical research: atmospheres*, vol. 112, no. D9, 2007.

[6] J. Haase, M. Ge, H. Vedel, and E. Calais, "Accuracy and variability of GPS tropospheric delay measurements of water vapor in the western Mediterranean," *Journal of Applied Meteorology*, vol. 42, no. 11, pp. 1547–1568, 2003.

[7] T. Hadas, F. N. Teferle, K. Kazmierski, P. Hordyniec, and J. Bosy, "Optimum stochastic modeling for GNSS tropospheric delay estimation in real-time," *GPS solutions*, vol. 21, pp. 1069–1081, 2017.

[8] D. Hogg, F. Guiraud, and M. Decker, "Measurement of excess radio transmission length on earth-space paths," *Astronomy and Astrophysics, vol. 95, no. 2, Mar. 1981, p. 304-307.*, vol. 95, pp. 304–307, 1981.

[9] G. Resch, "Water vapor radiometry in geodetic applications," in *Geodetic Refraction: Effects of Electromagnetic Wave Propagation Through the Atmosphere*. Springer, 1984, pp. 53–84.

[10] M. Bevis, S. Businger, T. A. Herring, C. Rocken, R. A. Anthes, and R. H. Ware, "GPS meteorology: Remote sensing of atmospheric water vapor using the global positioning system," *Journal of Geophysical Research: Atmospheres*, vol. 97, no. D14, pp. 15 787–15 801, 1992.

[11] M. Bevis, S. Businger, S. Chiswell, T. A. Herring, R. A. Anthes, C. Rocken, and R. H. Ware, "GPS meteorology: Mapping zenith wet delays onto precipitable water," *Journal of Applied Meteorology (1988-2005)*, pp. 379–386, 1994.

[12] H. Vedel, K. Mogensen, and X.-Y. Huang, "Calculation of zenith delays from meteorological data comparison of NWP model, radiosonde and GPS delays," *Physics and chemistry of the earth, part A: solid earth and geodesy*, vol. 26, no. 6-8, pp. 497–502, 2001.

[13] S.-W. Lee, J. Kouba, B. Schutz, D. H. Kim, and Y. J. Lee, "Monitoring precipitable water vapor in real-time using global navigation satellite systems," *Journal of geodesy*, vol. 87, pp. 923–934, 2013.

[14] C. Rocken, T. Van Hove, and R. Ware, "Near real-time GPS sensing of atmospheric water vapor," *Geophysical research letters*, vol. 24, no. 24, pp. 3221–3224, 1997.

[15] R. H. Ware, D. W. Fulker, S. A. Stein, D. N. Anderson, S. K. Avery, R. D. Clark, K. K. Droegemeier, J. P. Kuettner, J. B. Minster, and S. Sorooshian, "SuomiNet: A real-time national GPS network for atmospheric research and education," *Bulletin of the American Meteorological Society*, vol. 81, no. 4, pp. 677–694, 2000.

[16] A. Karabatić, R. Weber, and T. Haiden, "Near real-time estimation of tropospheric water vapour content from ground based GNSS data and its potential contribution to weather now-casting in Austria," *Advances in Space Research*, vol. 47, no. 10, pp. 1691–1703, 2011.

This article has been accepted for publication in IEEE Journal of Selected Topics in Applied Earth Observations and Remote Sensing. This is the author's version which has not been fully e
content may change prior to final publication. Citation information: DOI 10.1109/JSTARS.2024.3381792

[17] G. V. Bennitt and A. Jupp, “Operational assimilation of GPS zenith total delay observations into the Met Office numerical weather prediction models,” *Monthly Weather Review*, vol. 140, no. 8, pp. 2706–2719, 2012.
[18] G. Elgered, H. Plag, H. Van der Marel, S. Barlag, and J. Nash, “Exploitation of ground-based GPS for operational numerical weather prediction and climate applications.” COST, 2005.
[19] H. Vedel, S. de Haan, J. Jones, G. Bennitt, and D. Offiler, “E-GVAP third phase,” in *EGU General Assembly Conference Abstracts*, 2013, pp. EGU2013–10 919.
[20] M. Hernández-Pajares, J. M. Juan, J. Sanz, O. L. Colombo, and H. Van Der Marel, “A new strategy for real-time integrated water vapor determination in WADGPS Networks,” *Geophysical Research Letters*, vol. 28, no. 17, pp. 3267–3270, 2001.
[21] T. Iwabuchi, C. Rocken, Z. Lukes, L. Mervart, J. Johnson, and M. Kanzaki, “PPP and network true real-time 30 sec estimation of ZTD in dense and giant regional GPS network and the application of ZTD for nowcasting of heavy rainfall,” in *Proceedings of the 19th International Technical Meeting of the Satellite Division of The Institute of Navigation (ION GNSS 2006)*, 2006, pp. 1902–1909.
[22] J. Zumberge, M. Heflin, D. Jefferson, M. Watkins, and F. Webb, “Precise point positioning for the efficient and robust analysis of GPS data from large networks,” *Journal of geophysical research: solid earth*, vol. 102, no. B3, pp. 5005–5017, 1997.
[23] G. Gendt, G. Dick, C. Reigber, M. Tomassini, Y. Liu, and M. Ramatschi, “Near real time GPS water vapor monitoring for numerical weather prediction in Germany,” *Journal of the Meteorological Society of Japan. Ser. II*, vol. 82, no. 1B, pp. 361–370, 2004.
[24] X. Li, G. Dick, M. Ge, S. Heise, J. Wickert, and M. Bender, “Real-time GPS sensing of atmospheric water vapor: Precise point positioning with orbit, clock, and phase delay corrections,” *Geophysical Research Letters*, vol. 41, no. 10, pp. 3615–3621, 2014.
[25] Y. Yuan, K. Zhang, W. Rohm, S. Choy, R. Norman, and C.-S. Wang, “Real-time retrieval of precipitable water vapor from GPS precise point positioning,” *Journal of geophysical research: atmospheres*, vol. 119, no. 16, pp. 10 044–10 057, 2014.
[26] D. Odijk, B. Zhang, A. Khodabandeh, R. Odolinski, and P. J. Teunissen, “On the estimability of parameters in undifferenced, uncombined GNSS network and PPP-RTK user models by means of S-system theory,” *Journal of Geodesy*, vol. 90, no. 1, pp. 15–44, 2016.
[27] T. Liu, Y. Yuan, B. Zhang, N. Wang, B. Tan, and Y. Chen, “Multi-GNSS precise point positioning (MGPPP) using raw observations,” *Journal of geodesy*, vol. 91, pp. 253–268, 2017.
[28] F. Zhou, D. Dong, W. Li, X. Jiang, J. Wickert, and H. Schuh, “GAMP: An open-source software of multi-GNSS precise point positioning using undifferenced and uncombined observations,” *GPS solutions*, vol. 22, pp. 1–10, 2018.
[29] Y. E. Bar-Sever, P. M. Kroger, and J. A. Borjesson, “Estimating horizontal gradients of tropospheric path delay with a single GPS receiver,” *Journal of Geophysical Research: Solid Earth*, vol. 103, no. B3, pp. 5019–5035, 1998.
[30] J. Böhm, A. Niell, P. Tregoning, and H. Schuh, “Global Mapping Function (GMF): A new empirical mapping function based on numerical weather model data,” *Geophysical research letters*, vol. 33, no. 7, 2006.
[31] H. Ma, Q. Zhao, S. Verhagen, D. Psychas, and H. Dun, “Kriging interpolation in modelling tropospheric wet delay,” *Atmosphere*, vol. 11, no. 10, p. 1125, 2020.
[32] R. B. Langley, “GPS receiver system noise,” *GPS world*, vol. 8, no. 6, pp. 40–45, 1997.
[33] G. Marut, T. Hadas, J. Kaplon, E. Trzcina, and W. Rohm, “Monitoring the water vapor content at high spatio-temporal resolution using a network of low-cost multi-GNSS receivers,” *IEEE Transactions on Geoscience and Remote Sensing*, vol. 60, pp. 1–14, 2022.
[34] J. Böhm, G. Möller, M. Schindelegger, G. Pain, and R. Weber, “Development of an improved empirical model for slant delays in the troposphere (GPT2w),” *GPS solutions*, vol. 19, pp. 433–441, 2015.
[35] J. Davis, T. Herring, I. Shapiro, A. Rogers, and G. Elgered, “Geodesy by radio interferometry: Effects of atmospheric modeling errors on estimates of baseline length,” *Radio science*, vol. 20, no. 6, pp. 1593–1607, 1985.
[36] J. W. Marini, “Correction of satellite tracking data for an arbitrary tropospheric profile,” *Radio Science*, vol. 7, no. 2, pp. 223–231, 1972.
[37] T. Herring, “Modeling atmospheric delays in the analysis of space geodetic data,” *Proceedirws of Refraction of Transatmospheric simals in Geodesy, eds. JC De Munck and TA Spoelstra, Netherlands Geodetic Commission Publications on Geodesy*, vol. 36, no. 4, 1992.
[38] J. Böhm, B. Werl, and H. Schuh, “Troposphere mapping functions for GPS and very long baseline interferometry from European Centre for Medium-Range Weather Forecasts operational analysis data,” *Journal of geophysical research: solid earth*, vol. 111, no. B2, 2006.
[39] J. Böhm, G. Möller, M. Schindelegger, G. Pain, and R. Weber, “Development of an improved empirical model for slant delays in the troposphere (GPT2w),” *GPS solutions*, vol. 19, pp. 433–441, 2015.
[40] A. E. Niell, “Global mapping functions for the atmosphere delay at radio wavelengths,” *Journal of geophysical research: solid earth*, vol. 101, no. B2, pp. 3227–3246, 1996.
[41] J. Saastamoinen, “Atmospheric correction for the troposphere and stratosphere in radio ranging satellites,” *The use of artificial satellites for geodesy*, vol. 15, pp. 247–251, 1972.
[42] P. Li, X. Zhang, M. Ge, and H. Schuh, “Three-frequency BDS precise point positioning ambiguity resolution based on raw observables,” *Journal of Geodesy*, vol. 92, pp. 1357–1369, 2018.
[43] F. Zhou, D. Dong, P. Li, X. Li, and H. Schuh, “Influence of stochastic modeling for inter-system biases on multi-GNSS undifferenced and uncombined precise point positioning,” *GPS solutions*, vol. 23, pp. 1–13, 2019.
[44] R. Wang, D. Becker, and T. Hobiger, “Stochastic modeling with robust Kalman filter for real-time kinematic GPS single-frequency positioning,” *GPS Solutions*, vol. 27, no. 3, p. 153, 2023.
[45] X. Li, J.-P. Barriot, Y. Lou, W. Zhang, P. Li, and C. Shi, “Towards millimeter-level accuracy in gnss-based space geodesy: A review of error budget for gnss precise point positioning,” *Surveys in Geophysics*, pp. 1–90, 2023.
[46] E. Trzcina, D. Tondaś, and W. Rohm, “Cross-comparison of meteorological parameters and ztd observations supplied by microwave radiometers, radiosondes, and gnss services,” *Geodesy and Cartography*, vol. 70, no. 2, 2021.
[47] W. J. Riley and D. A. Howe, “Handbook of frequency stability analysis,” 2008.

V. Biography Section

Rui Wang received the dual B.S. degree from the University of Stuttgart, Germany, and the Wuhan University, China, in 2018; the M.S. degree in Geodesy and Geoinformatics from the University of Stuttgart in 2019. Since November 2019, she has been as a research associate and also a Ph.D. candidate at the Institute of Navigation, University of Stuttgart. Currently, she focuses on GNSS positioning and atmospheric corrections for satellite navigation.

Grzegorz Marut received the M.Sc. degree in geoinformatics from the Wrocław University of Environmental and Life Sciences (UPWr), Wrocław, Poland, in 2021. He is currently pursuing the Ph.D. degree. He is developing novel models for processing GNSS observations from low-cost receivers. His master's thesis was awarded by the Polish Space Agency and the Polish Ministry of Development and Technology.

This article has been accepted for publication in IEEE Journal of Selected Topics in Applied Earth Observations and Remote Sensing. This is the author's version which has not been fully e
content may change prior to final publication. Citation information: DOI 10.1109/JSTARS.2024.3381792

Tomasz Hadaś received his Ph.D. degree in satellite geodesy from the UPWr in 2015 and is currently an Associate Professor with the UPWr. He was a laureate of the Minister's scholarship for outstanding young scientists in Poland (2018) and a Marie Skłodowska-Curie fellow at the Institute of Navigation of the University of Stuttgart, Germany (2019-2021). He focuses on real-time mulit-GNSS precise positioning and troposphere remote sensing with GNSS.

Thomas Hobiger received the M.S. and Ph.D. degrees in geodesy and geophysics from the Vienna University of Technology, Vienna, Austria, in 2002 and 2005, respectively. He is a Full Professor with the University of Stuttgart, Germany, where he is the head of the Institute of Navigation. His main research focuses on positioning, navigation and timing and he has been involved in projects related to autonomous aircraft, GNSS, GNSS-R, software-defined radio, precise orbit determination, high-performance computing, propagation of radio waves, and time and frequency transfer. Prof. Hobiger is an IAG Fellow and was a recipient of the AGU Geodesy Section Award, in 2018. He was also a recipient of the Tsuboi Award, the EPS Award 2010, and the EGU Outstanding Young Scientist Award 2011.